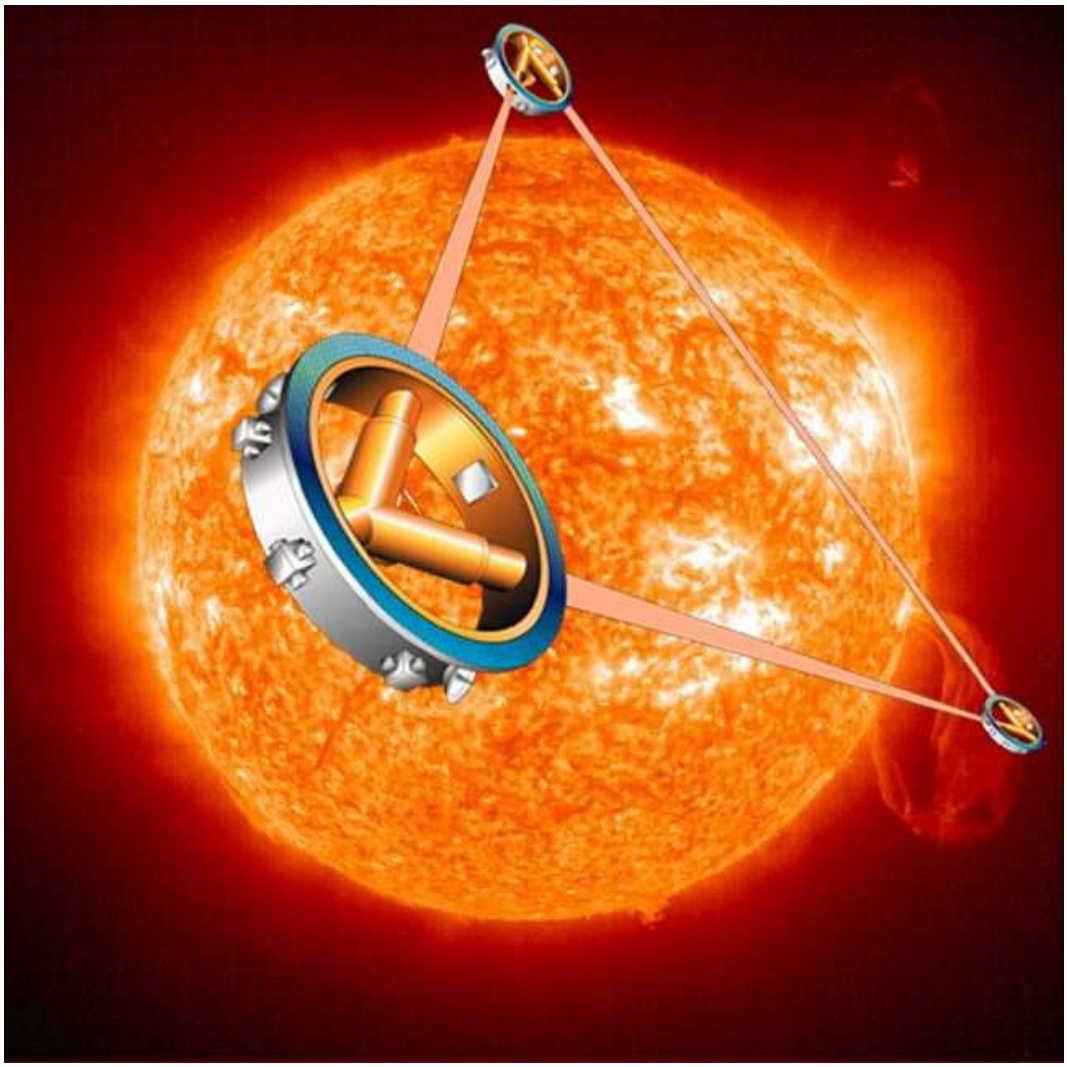

PHOEBUS

PHysics Of Events BUrsted by the Sun

PHOEBUS

PHysics Of Events BUrsted by the Sun

on

LISA

Catia Grimani[1] **& Helios Vocca**[2]

1 University of Urbino and INFN Florence, Via S. Chiara, 61029, Urbino, Italy

2 University and INFN Perugia, Via A. Pascoli, 06100, Perugia, Italy

TABLE OF CONTENTS

1. Introduction 1

2. Preliminary notes 3

3. Latitude dependence of energetic solar and cosmic-ray particles 6

4. Longitude dependence of solar energetic particles 9

5. LISA orbit characteristics 11

6. Particle monitors on LISA 13

7. Solar physics with LISA 15

7.1 Introduction 15

7.2 Expected proton fluence during the LISA mission 17

7.3 Solar energetic proton flux modelization 17

7.4 LISA particle monitor expected response to SEPs 28

7.5 Solar energetic particle mapping 29

8. Space wheather 32

8.1 Introduction 32

8.2 Space weather with LISA 34

9. Network with other space weather experiments 35

10. Fake gravitational wave signals induced on LISA by CMEs 36

Acknowledgments 36

References 38

1 Introduction

The LISA (Laser Interferometer Space Antenna) experiment is devoted to gravitational wave detection in space in the frequency range 10^{-4} - 10^{-1} Hz. The sensitivity goal that LISA is supposed to achieve is about 4×10^{-21} $1/\sqrt{\text{Hz}}$ at 3 mHz.

LISA consists of three spacecraft located at the corners of an equilateral triangle of 5×10^{6} km side. The spacecraft form a giant Michelson interferometer with a third arm allowing us to gather independent information on the two gravitational wave polarizations and for redundancy. The center of the triangle is on the ecliptic plane, 20° behind the Earth. The three spacecraft rotate about the center of the formation in the plane of the triangle that is inclined at 60° with respect to the ecliptic plane (see http://lisa.jpl.nasa.gov/WHATIS/mission2.html). One rotation lasts one year.

Each spacecraft hosts optical telescopes and two inertial sensors. The heart of the inertial sensors is a cubic Pt/Au test mass constituting the mirrors of the Michelson interferometer.

The spacecraft shield the test masses by external noise and it is maintained always centered with respect to them by a drag-free control system. Capacitive sensing in three dimensions is used to measure the displacements of the proof masses relative to the spacecraft.

Cosmic rays with energies larger than 100 MeV(/n) are able to penetrate and charge the test masses, generating spurious Coulomb forces between the test masses and the surrounding electrodes that might mimic gravitational wave signals. Consequently, the test masses must be periodically discharged by using beams of ultraviolet light. In order to do that correctly, the test-masses charging will be monitored through particle counters located on board each spacecraft. A silicon telescope has been designed and it will be located on board the LISA Pathfinder mission (Lobo, 2004).

Lisa is expected to be launched in 2011. The nominal mission lifetime is 2 years with a possibility to extend it up to 10 years.

We propose to use the onboard particle counters to map the transit of

Solar Energetic Particles (SEPs) correlated to strong Coronal Mass Ejections (CMEs) through the LISA spacecraft at various steps in longitude: 2 degrees among spacecraft, 20 degrees among LISA and experiments orbiting near Earth and, eventually, different intervals if data from other experiments in space will be available.

These measurements are of interest to solar physics and space weather since SEPs endenger astronaut health and space equipments.

CME occurrence time, SEP flux trend and fluence intensity prediction of individual events represents an impossible challange at present time.

A correct modelization of evolving CMEs represents a first, fundamental step forward.

2 Preliminary notes

The Sun flings 10^6 tons of fully ionized plasma from the corona out into the space every second. This material constitutes the solar wind (fig.1). Solar wind particles (mainly electrons and protons) travel at supersonic speeds of 200-800 km/s. Near the Earth the solar wind plasma has a density ranging between 0.4 and 100 particles/cm^3 with an average value of 6 particles/cm^3. Typical particle energies range between 0.5 and 3 keV (Reames, 2003). The expanding solar wind drags also the solar magnetic field outward, forming what is called the interplanetary magnetic field. Although the solar wind moves out almost radially from the Sun, both solar wind and magnetic field are twisted into a spiral by the Sun rotation (fig.2).

At the orbit of the Earth the angle between the field lines and the radial is about 45°. The value of the interplanetary magnetic field ranges between 0.2 and 80 nT with an average value of 6 nT. Sectors (typically four) with alternating inward and outward directed magnetic fields can be identified (fig.3).

In addition to the solar wind which blows continuously, much more energetic electrons and protons (solar energetic particles with energies larger than 1 MeV) generated by impulsive or gradual solar flares can reach the Earth.

After 1977 (Pallavicini et al., 1977) the rate of occurrence of solar flares has been modelled on the basis of the characteristics of soft X-ray emissions (see for example Wheatland, 2000). In principle, it would also be possible to order the solar energetic events through the observation of the occurrence of hard X-ray emissions or SEP fluence reaching the Earth. As a consequence, some confusion about flare rate and characteristics may occur. Short duration events are more properly indicated as 'solar flares' while long duration events are thought to be associated with 'Coronal Mass Ejections' . CMEs are believed to be caused by sudden disruptions in the Sun's magnetic field. These magnetic field lines are supposed to stretch until they breake. Large CMEs can contain 1000 tons of matter that can reach speeds at the Earth of up to 2000 km/s.

The characteristics of impulsive and long duration events are reported in Table 1.

It has to be stressed that only 1-2% of CMEs (fast CMEs driven shocks)

Table 1: Properties of Impulsive and Gradual Solar Events

	Impulsive	Gradual
Particles:	Electron-rich	Proton-rich
^{3}He/^{4}He	about 1	about 0.0005
Fe/O	about 1	about 0.1
H/He	about 10	about 100
Q_{Fe}	about 20	about 14
Duration	Hours	Days
Longitude Cone	40-70 deg peak at 60	more flat - 20 deg uncertainty
Radio Type	III,V(II)	II,IV
X-rays	Impulsive	Gradual
Coronagraph	-	CME (96%)
Solar Wind	-	IP Shock
Events/y	about 1000	about 10

produce SEPs.

In gradual events no element is completely ionized and the charge for iron, for example, is 14±1 on average. The events ^{3}He rich are characterized by an ionization state for iron of 20.5±1.2. This evidence indicates that gradual events consist of coronal material (about 2 MK) while impulsive events are flare-heated (about 10 MK).

Pure impulsive or gradual events are rare.

On short time scales of the order of the duration of the event, the particle fluxes rise over a period of 1/2-1 day with a slow decay of about few days. A strong increase after a first decay phase is found in the largest events and is due to a series of CMEs and shocks. The majority of solar proton events occurs during years 5-8 of the solar cycle (Shea and Smart, 2001). It has to be underscored that in most cases SEPs present energies smaller than 10 GeV even if observations of particles with energies as high as 50 GeV and more have been reported. In particular, in Karpov et al., 1997 integral proton intensities (about 10^{-5} cm^{-2} s^{-1} sr^{-1}) at energies $E_p \geq 500$ GeV are found [1]

[1]Protons above 500 GeV were detected after 2 days from the arrival of the bulk of the other relativistic ones

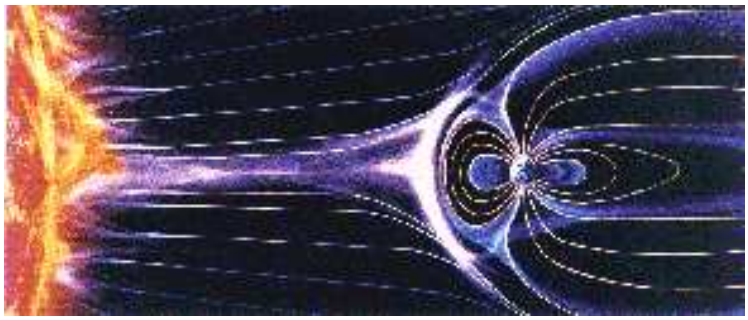

Figure 1: Artistic view of the solar wind and the Earth magnetosphere. *http://www.windows.ucar/edu/tour/link=/glossary/images/solar_ wind_ gif _ image.html*

for the September 29 1989; June 15, 1991 and October 12, 1981 GLEs (Ground Level Events). Often impulsive-flare events cluster in or behind a CME where magnetic field lines connect to a solar active region where flares are occurring. In most cases a particle velocity dispersion can be observed when particles arrive in inverse order to their velocity. Particles from a large, magnetically well connected gradual event, associated with a CME-driven shock, also show velocity dispersion early in the event but present identical time profiles that last for several days late in the event. The energy content in impulsive events appears to lie below 1 MeV (Reames, Kahler and Ng, 1997).

The most energetic particles (energies larger than 1 GeV) arrive with a delay of only a few minutes after the visual recognition of the flare. Lower energy particles appear in increasing numbers while the high energy particles fade away.

Since no particles with energies smaller than 100 MeV(/n) will be monitored by the LISA counters, we are interested in the rate of occurrence of those solar events able to generate particles above this energy. As these events are characterized by protons overcoming any other kind of particle by more than one order of magnitude, we focus our study on protons only.

In paragraph 7.2 we report the proton fluences expected during the LISA mission (Nymmik, 1999). We recall here that the omnidirectional flux above 10 MeV for each solar cycle during the last three solar cycles is of a few units 10^{10}.

Single event fluences of protons above 10 MeV larger than 1.5 10^9 protons/cm^2

are very rare. There having been only 14 since 1963.

Between August 1972 and October 1989 there were no events larger than 10^{10} protons/cm^2.

The archimedian spiral pattern of the interplanetary magnetic field generates an asymmetry in the intensity-time profiles of SEP events from eastern and western longitudes on the Sun. In particular, events originating in the western hemisphere of the Sun are more likely to produce solar particles able to reach the Earth and LISA with respect to those flares in the eastern hemisphere. The properties of SEP profiles are explained in terms of direct magnetic connection between the shock and the detecting spacecraft. The time of the onset corresponds to the time at which the shock intercepts the magnetic field lines to the spacecraft plus the particle travel time to the spacecraft. The time of the maximum is thought to indicate the time at which the spacecraft is connected to the part of the shock which accelerates particles more efficiently. The nose of the shock is assumed to be a more efficient accelarator with respect to its flanks.

For many years all our knowledge on solar phenomena was acquired from the viewpoint of the Earth that moves between $\pm 7.25^o$ of the solar latitude. In the last fifteen years the Ulysses experiment and other spacecraft orbiting near Earth have given precious hints on SEP characteristics as a function of solar latitude, longitude and distance from the Sun.

3 Latitude dependence of energetic solar and cosmic-ray particles

The Ulysses experiment has explored the inner heliosphere since its launch in 1990. Between 2000 and 2001 it has passed from the South to the North poles of the Sun revealing latitudinal structure of cosmic-ray modulation and solar energetic particle populations during a period of solar maximum. While latitude gradients were found in galactic cosmic rays at solar minimum (see for example Grimani et al., 2004 and references therein) no latitude effects were detected at solar maximum. Increases in particle fluxes at tens of MeV due to flares and CMEs were detected often. Simultaneous high latitude and near-

Figure 2: Artistic view of the interplanetary magnetic field. *http://pluto/space/swri.edu/image/glossary/imf.html*

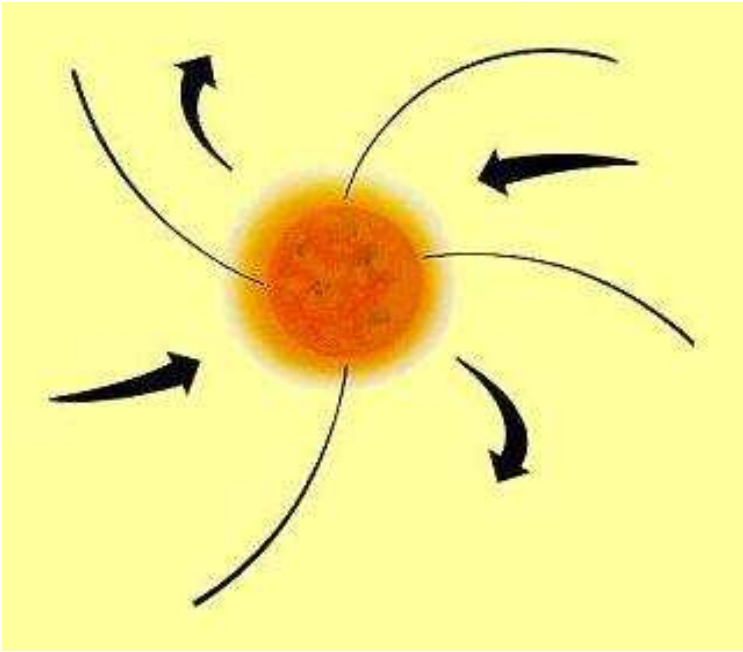

Figure 3: Interplanetary magnetic field sectors.

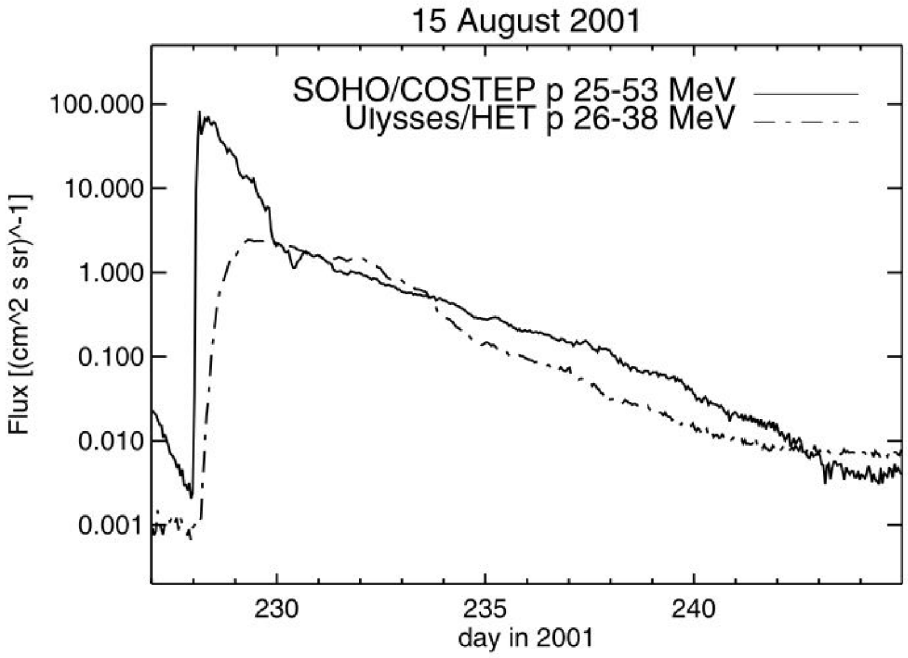

Figure 4: SEP fluxes at different latitudes. Figure from Dalla et al., 2003

Earth observations show that most events that produce large flux increases near Earth also produce flux increases at Ulysses. It can be concluded that primary and solar cosmic-ray observations are consistent with transport of energetic particles between the equatorial and polar regions and across the interplanetary magnetic field in the inner heliosphere (McKibben et al., 2003). As an example, an important latitude effect has been found by Dalla et al., 2003 where a comparison between SEP fluxes (gradual event) measured at Ulysses at a latitude of 63° N and distance from the Sun of 1.63 AU and at SOHO in the ecliptic at 1 AU has been carried out (fig.4).

The peak intensity at high latitude is typically smaller than in the ecliptic and it is reached at a later time. The decay phase is characterised by similar decay time constants at the two locations.

4 Longitude dependence of solar energetic particles

A study of the longitude dependence of the spatial and temporal distribution of SEPs has been debated in Reames, Barbier & Ng, 1996; Reames, Kahler & Ng, 1997. SEP flux measurements ranging between a few and a few hundreds MeV from three different satellites (Helios 1, Helios 2 and IMP8) have been carried out for various gradual events.

Simultaneous observations on various spacecraft separated in longitude allow us to study the distribution of energetic particles around an evolving CME-driven shock. Time profiles of 1-10 MeV protons are affected by the evolution of the intersection point between the observer magnetic field line and the shock. This point sweeps rapidly eastward across the face of the shock with time at a rate of 27°-45° day^{-1} compared to solar rotation of 13° day^{-1}. We recall that The stronger acceleration occurs near the nose of the shock while the shock strength and the acceleration weaken around toward either flank. Small shock CMEs are expected to cause rapid changes in intensity. Large CME shocks might generate flat longitude profiles in even widely separated spacecraft. As an example, fig. 5 shows time-intensity profiles of protons between 3 and 6 MeV as a function of longitude about a CME as shown in the inset (Reames, Kahler & Ng, 1997).

Helios 1 passed near the nose of the shock and observed a flat profile followed by a peak at the shock. Helios 2 and IMP 8 farther around the west flank detected increasingly slower rises. This particular event has a relatively narrow span in longitude; other events present higher intensities over more than 90° interval in longitude with respect to the east and west of the central longitude of the CME.

Fig. 5 also shows that the intensities measured at the three spacecraft are comparable, within a factor of $\simeq 2$, late in the event, long after shock passage. This is a region of spatially and temporally invariant spectra (see fig. 6 - Reames, Kahler, and Ng, 1997).

At energies above about 10 MeV the time profiles are also affected by decreases in the acceleration efficiency with time as the shock strength decreases

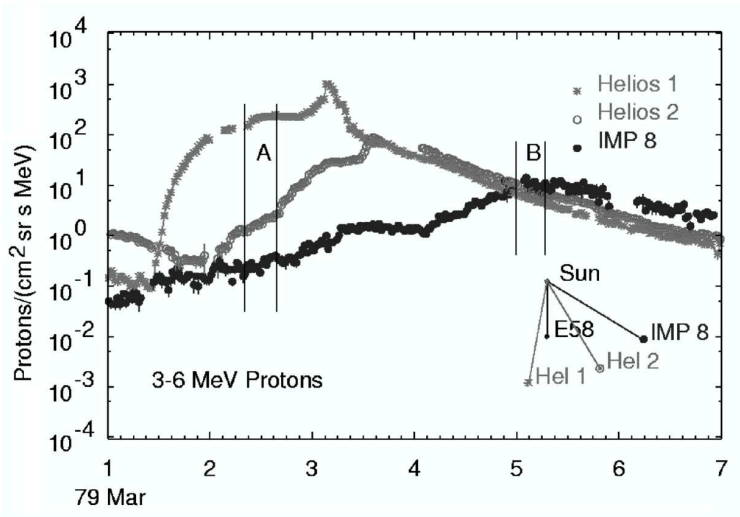

Figure 5: Time-intensity profiles for 3 - 6 MeV protons observed by spacecraft at different longitudes (see inset). Figure is taken from Reames, Kahler & Ng, 1997. Time periods A and B indicate longitude dependent fluxes and space invariant observations, respectively.

at least as fast as r^{-2}. The radius where shock fails to produce saturation in particle intensity at a given energy, also depends upon longitude and upon the initial shock strength. In moderate events protons maintain near-maximum intensity until the shock reaches about 0.5 AU. Ten GeV protons peak near the Sun at 0.05 AU. The outward speeds of these CMEs reach 2000 km s^{-1} (Kahler, 1994; Reames, Barbier & Ng, 1996). For particles in the GeV range, the most effective longitude is 60° W (Smart & Shea, 1996). CME shock impact the Earth when the associated solar activity ranges mainly between about 60° E and 120° W (Shea & Smart, 2001).

The lack of longitude dependence of intensities at all energies late in the event, well behind the shock is in contrast with the dramatic longitude dependence ahead of the shock. Nearly identical spectra are seen over longitude intervals of up to 160° and the intensities at all energies decline with e-folding from constants of 6-18 hr for periods of about 3 days (Reames, Kahler & Ng, 1997). The region of the invariant spectra is associated with acceleration on the eastern flank of the shock wave driven out from the Sun by a CME. On the western flank of the shock the SEP event is more dynamic. For well connected western SEP events (on the eastern flank of the shock), invariant spectra are

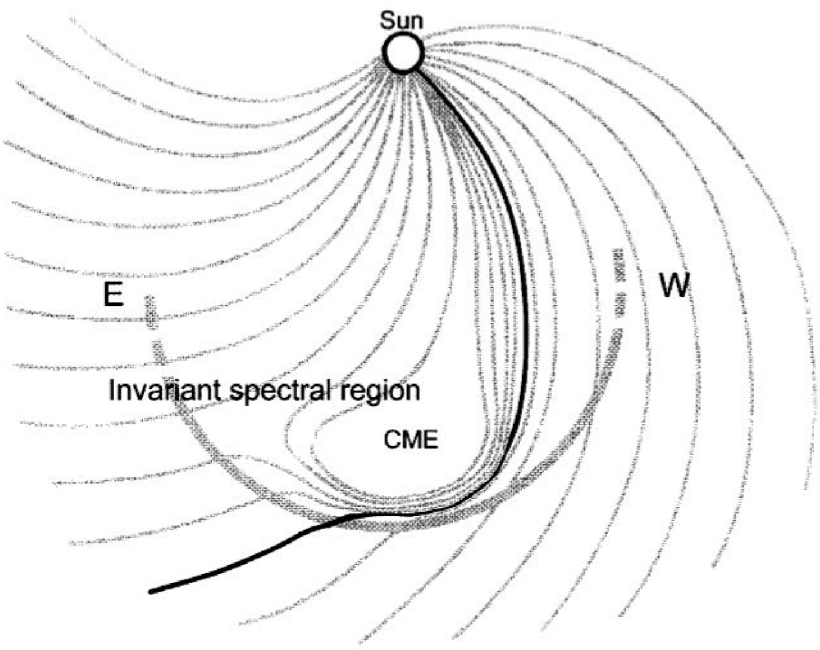

Figure 6: SEP invariant spectral region (figure from Reames, Kahler & Ng, 1997)

seen up to a day before shock arrival and continue through the reminder of the event. For central and eastern SEP events (western flank of the shock), invariance begins after shock passage but usually before the spacecraft passes through the region we associate with the CME itself. Even spacecraft far around on the western flank of the shock eventually see invariant spectra well after shock transit.

In fig.7 SEP observations up to a few tens of MeV at various longitudes and a modelization of an evolving CME are reported.

The description of the particle flux acceleration due to an evolving CME-driven shock must be revised in case of a new CME propagating inside a previous one (fig.8).

5 LISA orbit characteristics

The LISA orbit is presented in fig.9. Each spacecraft is located 5×10^6 km away from the others, and about 50×10^6 km behind the Earth. The orbit of

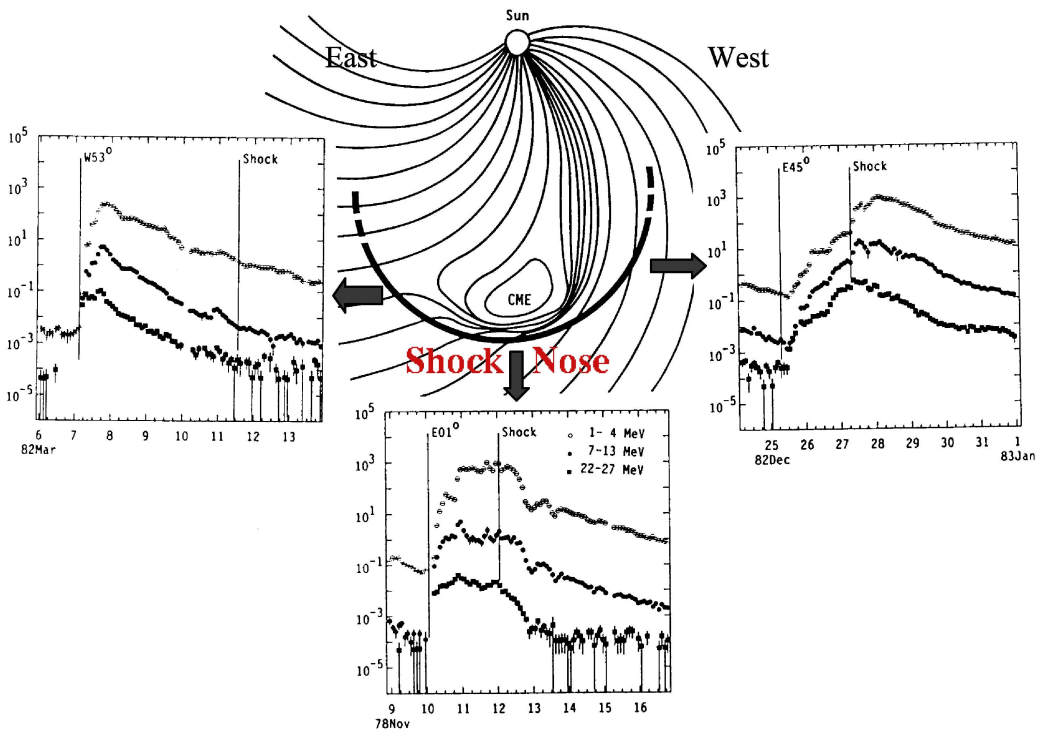

Figure 7: SEP observations at different longitudes and modelization of a propagating CME. Figure from Reames, 2002.

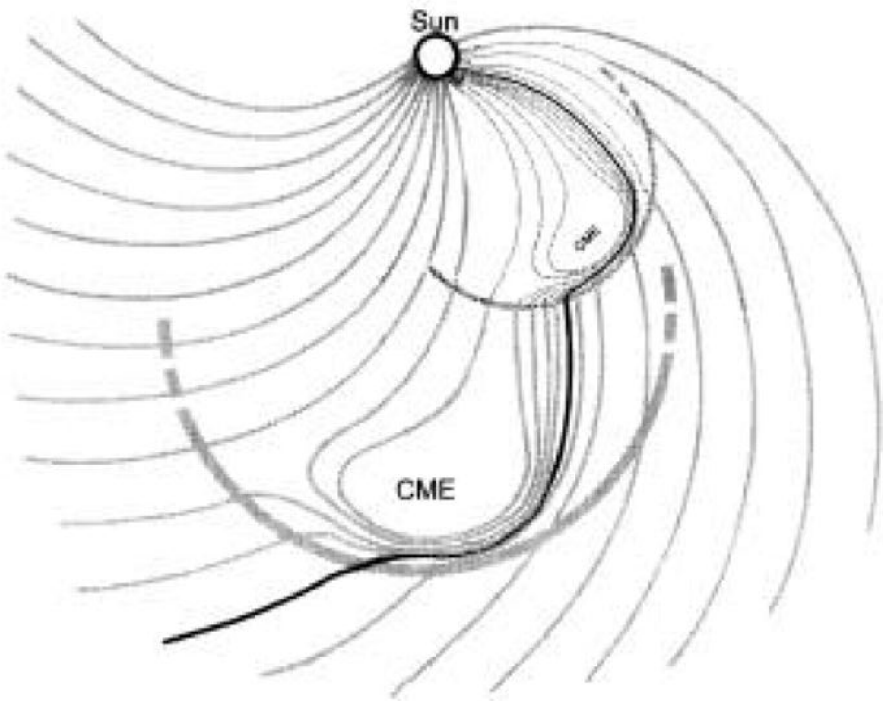

Figure 8: Modelization of propagating CMEs (figure from Reames, 2002).

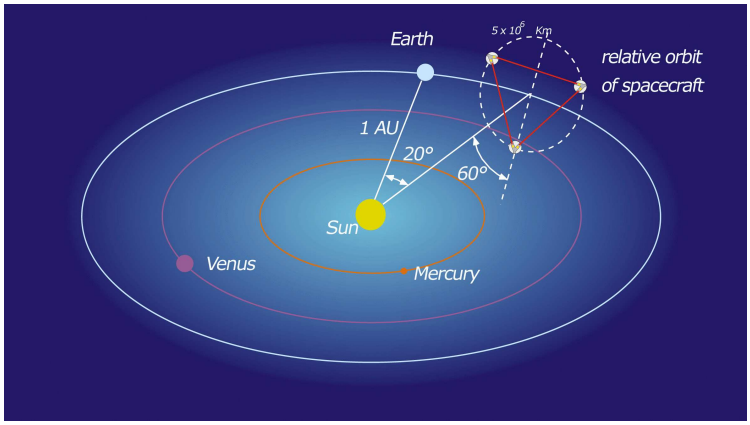

Figure 9: LISA orbit around the Earth.*http://lisa.jpl.nasa.gov/gallery.html*

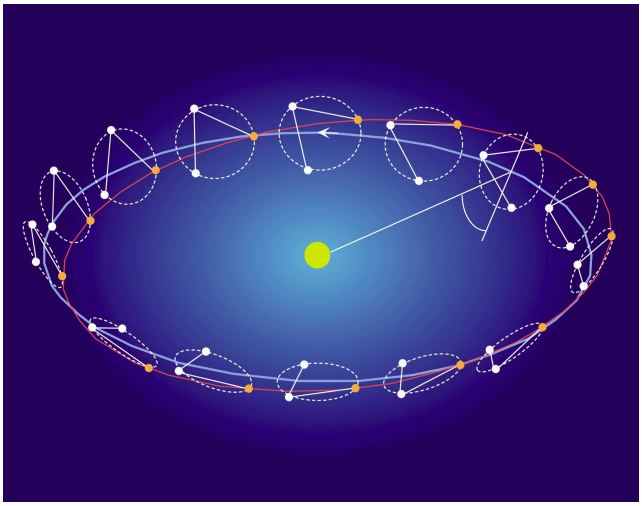

Figure 10: LISA spacecraft trajectory.*http://lisa.jpl.nasa.gov/gallery.html*

individual spacecraft is shown in fig.10.

Spacecraft minimum and maximum radial distance from the Sun, latitude off the ecliptic plane and longitude with respect to Earth have been reported in Table 2 . It can be noticed that the three spacecraft of the LISA experiment present heliolatitudes differing by less than 1° from that of the Earth and heliolongitudes varying between 19° and 21° with respect to that of the Earth.

6 Particle monitors on LISA

Several measurements of galactic cosmic-ray spectra in all solar modulation conditions are available in literature (see for example Grimani et al., 2004; Stephens & Streitmatter, 2001; Grimani et al., 2002). Consequently, it is

Table 2: LISA spacecraft orbit characteristics

Distance from the Sun	$149 \div 152 \cdot 10^6$Km $(0.9933 \div 1.0133 AU)$
Latitude off the ecliptic	$0.7^o \div 1.0^o$
Longitude difference with respect to Earth	$19^o \div 21^o$

possible to estimate the background charging process of the LISA test masses due to galactic cosmic rays (see for example Araújo et al., 2004; Vocca et al., 2004; 2005; Grimani et al., 2005). It can be worth to remind that these estimates are characterized by uncertainties of 30% or more in normalization because of the spread among the whole set of available data well above 10 GeV. In addition to galactic cosmic rays, energetic particles of solar origin must be considered. These last ones can produce charge deposits in the test masses several orders of magnitude larger than those due to galactic cosmic rays. In Vocca et al., 2005 it has been shown that the experiment performance is limited in the lower frequency range by the occurrence of these events.

The test masses are surrounded by about 13 g/cm^2 of matter. Protons and nuclei below 100 MeV/n energy stop before reaching the masses.

Particle detectors will be located on board the LISA spacecraft in order to monitor the overall particle incident flux above 100 MeV(/n). To this purpose, a proper layer of Titanium (2.2 cm) will surround the particle detectors.

The project for the development, positioning and orientation of these telescopes for the Lisa Pathfinder mission is in progress (Lobo, 2004).

The design is basically the following: two rectangular silicon detectors will be located one in front of the other. Total count rate on one detector, coincidence between silicon layers and proton energy spectrum measurements up to a few hundreds of MeV will be available.

Two equal wafers of silicon detectors of 300 μm thickness will be located at 2 cm distance (Araújo & Wess, 2004). The dimensions of each silicon detector are 1.4×1.05 cm^2. The maximum particle counting before saturation is 10^8 protons s^{-1}.

The particle counter arrangement is shown in fig.11.

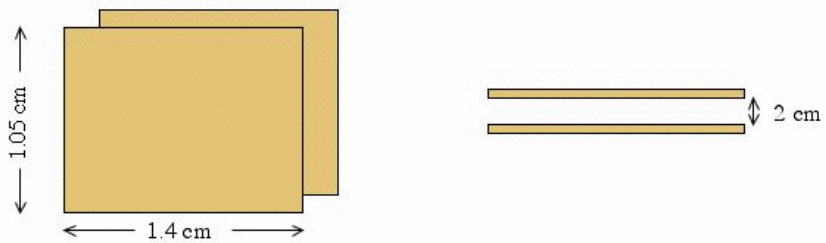

Figure 11: Sketch of the silicon telescope on LISA Path-Finder.

We will assume here that the same telescope arrangement developed for LISA Pathfinder will be used for LISA.

In the following paragraphs we present possible scenarios regarding the expected count rates on the particle detectors when different fluence SEP events driven by CMEs propagate through the LISA spacecraft.

7 Solar physics with LISA

7.1 Introduction

In spite of the random solar particle event occurrence, a higher probability is observed during periods of major solar activity. We recall that the first half of the LISA mission will occur at solar maximum. Often, the main concern for space experiments and astronaut health is related to cumulative exposure, being the typical energy range of interest for space weather 500 keV-100 MeV. SEPs are studied essentially below a few tens of MeV since only the most strong events produce particles with energies larger than 100 MeV able to

overcome galactic cosmic-ray fluxes.

The monitoring of the LISA test-mass charging, requires a different approach. Large events dominate the total fluence during a whole solar cycle while they occur for a minor period of time.

We have calculated the expected proton fluence for each year of the LISA mission. In particular, we have used the model developed by R. A. Nymmik (Nymmik, 1999) to estimate the expected number of SEP events with fluence larger than 10^6 protons cm^{-2} with energies larger than 30 MeV (paragraph 7.2).

We have also estimated at the occurrence of individual strong solar events the expected count rate detected by the particle telescopes onboard the LISA spacecraft.

A code for the characterization of SEP events at user-specified locations in space for the estimate of time-dependent proton fluxes and fluences for particle energies ranging between 10 and 100 MeV has been developed by Aran, Sanahuja & Lario (Aran, Sanahuja & Lario, 2003). Unfortunately, our measurements will be limited to higher energies and therefore, we cannot use their work. Very recently Sokolov et al. (Sokolov et al., 2004) have presented a model to simulate the time-dependent transport and diffusive acceleration of particles at shock waves driven by CMEs. In particular, they have estimated the upstream proton flux at the Earth. A maximum energy of 700 MeV for particles confined at the shock is found. The cut-off energies for those particle spectra are found at smaller values compared to those observed at the peak of the most strong events, however these incoming particles are very dangerous to instruments and manned missions in space. As a result, we have chosen to fit the observed solar energetic proton fluxes at 1 AU as a function of time for individual events of different fluences to estimate the count rate in our telescopes. A comparison among measured SEP fluxes and available modelization is made per peak fluxes. SEP fluxes observed as a function of time have been also compared to the upstream proton fluxes reported in the work by Sokolov et al., 2004.

The possibility to use the particle monitor on board LISA to study strong solar event dynamics was firstly reported in Grimani & Vocca, 2005.

7.2 Expected proton fluence during the LISA mission

In Nymmik, 1999, a model to estimate the SEP fluence distribution as a function of the solar activity is reported. Nymmik has found that the mentioned distribution follows a power-law function with an exponential steepening for large fluences. This model applies to solar proton fluences ranging between 10^6 and 10^{11} protons cm^{-2} for proton energies larger than 30 MeV. The results presented by Nymmik were inferred from the analysis of the spacecraft IMP-7 and 8 measurements of SEP events during the solar cycles 20-22 and from the proton fluxes indicated by the observations of radionuclides in lunar rocks generated in the last few million years.

We have estimated the expected number of SEP events in individual intervals of fluence during the LISA mission (2011 - 2021) accordingly to the following steps:

(i) we have found the number of SEP events, <n>, for each year of the LISA mission on the basis of the minimum and maximum predicted solar spot number (<w>) for the same period (see also Wess, Araújo and Sumner, 2003)

$$< n >= 0.0694 < w > \tag{1}$$

(ii) we have determined the normalization constant C by integrating the function

$$dn = C\phi^{-1.41}e^{-\phi/\phi_c}d\phi \tag{2}$$

and by equating it to the expected number of SEP events calculated in (i). ϕ_c has been assumed equal to 4×10^9.

(iii) Finally, after constant C determination, we have estimated the number of expected events per fluence interval. The results have been reported in figs. 12 and 13.

7.3 Solar energetic proton flux modelization

As we have stressed in the previous paragraphs, not much is known about SEP fluxes above 100 MeV(/n). The PHOEBUS measurements on LISA will allow us to obtain precious hints about SEP acceleration and transport phenomena.

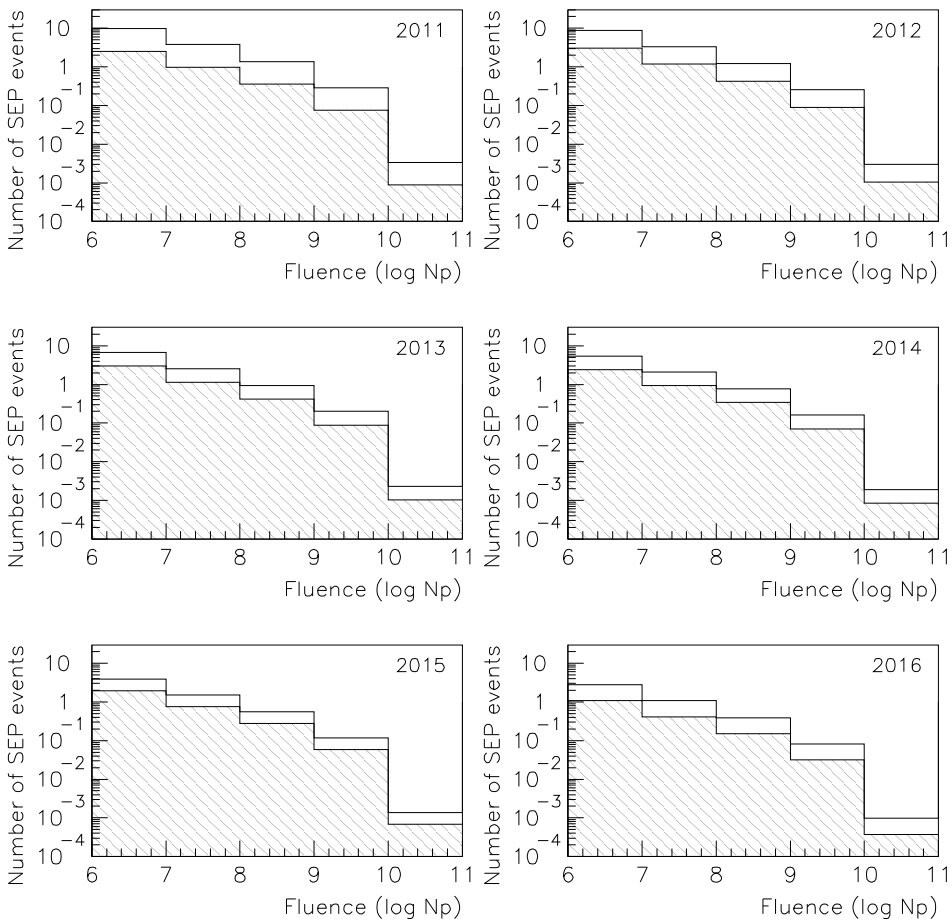

Figure 12: Maximum (white histograms) and minimum (dashed histograms) expected number of SEP events during the first part of the LISA mission versus fluence.

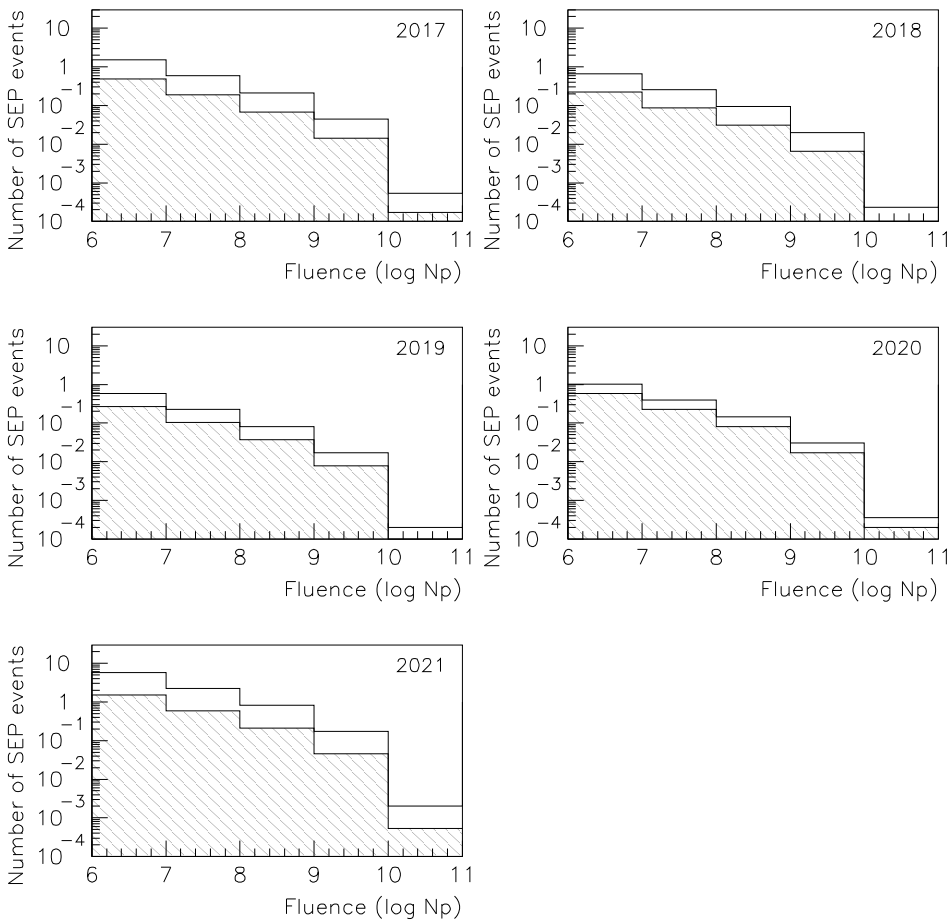

Figure 13: Maximum (white histograms) and minimum (dashed histograms) expected number of SEP events during the final part of the LISA mission versus fluence.

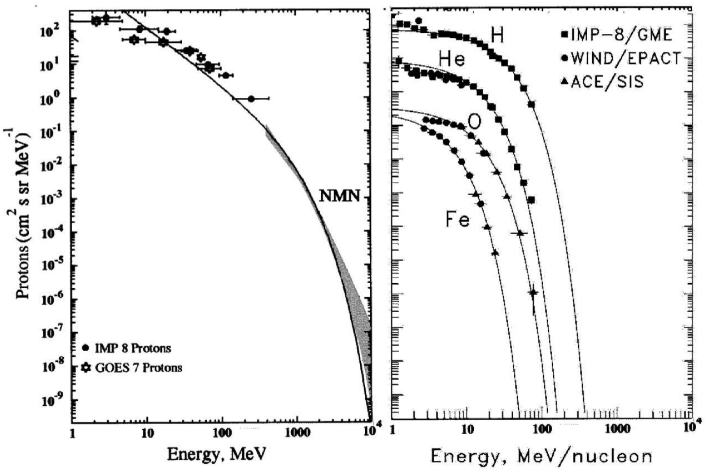

Figure 14: The proton energy spectrum in the 1989 September 29 SEP event (left panel) is measured by spacecraft and the neutron monitor network (NMR) [*Lovell, Duldig, and Humble* 1998]. The right panel shows spectra of ions in the 1998 April 20 event [*Tylka et al.* 2000]. Proton spectral knees occur at much different energies in the two events. Figure is taken from Reames, 2000.

Usually, the SEP energy differential flux J(E) is modelled as it follows (Aran, Sanahuja and Lario, 2003):

$$J(E) = j_o E^{-\gamma} \tag{3}$$

at a few MeV, while at higher energies the energy spectrum departs from the power-law trend and it shows an exponential cut-off forming a 'knee'.

$$J(E) = j_o E^{-\gamma} e^{-E/E_o} \tag{4}$$

where j_o is a normalization constant and E_o is an e-folding energy larger than 10 MeV.

Fig.14 shows examples of spectral knees in SEP events. The left panel shows proton data taken on spacecraft and measured by the ground-level neutron monitor network (NMN, shaded region in the figure) in the September 29th 1989 SEP event. The 'knee' of the spectrum is at an energy (E_{knee}) of about 1 GeV for this event (Lovell, Duldig, & Humble 1998). The right-hand panel in fig.14 shows spectra of H, He, O, and Fe in the 1998 April 20 event. In this event, E_{knee} is at about 15 MeV for protons and scales as Q/A for the other species. In other few observed events, the e-folding energy/nucleon does

not always scale linearly with Q/A (Tylka et al. 2000). It is difficult to understand the origin of this large difference in the energy of the spectral 'knees' for protons in the two events in fig.14. Both events occurred near the west limb of the Sun and the CME speeds were $\simeq$ 1800 and 1600 $km\ s^{-1}$ in the 1989 and 1998 events, respectively. The physical mechanism of shock acceleration that determines the knee energies is not well known. Moreover, many of the largest events have knee energies above the region where measurements were available.

The SEP particle flux time dependence has been reported in Grieder, 2004 as:

$$J(P,t) = I_o e^{-P/G(t)} \tag{5}$$

where P is the particle rigidity, I_o, measured in $cm^{-2}\ s^{-1}\ sr^{-1}$, is the (flare) parameter characterizing the flare intensity and G(t) represents the slope of the spectrum as a function of time. I_o varies between 2 and 1000 while G ranges between 40 and 400 MV. In fig. 1 of the paper Reames, 2001, the SEP intensity time profiles of six events have been reported in the energy intervals 8.7-14.5 MeV, 39-82 MeV and 100-500 MeV. It can be observed that, in general, the trend reported in equations (3) and (4) is respected, however some events can depart from above behaviour as a function of the solar longitude where the CMEs were generated with respect to the observer.

PHOEBUS on LISA will offer the possibility to map individual solar events at the same distance from the Sun but at different longitudes. The parameters of the above equations can be determined on the basis of the particle flux observations in correspondence of the three LISA spacecraft.

The peak fluxes of various fluence events have been studied by Mottl & Nymmik (Mottl & Nymmik, 2002 hereafter M&N).

In figs. 12 and 13 it is possible to notice that a few events per year are expected with fluences up to 10^9 protons/cm^2 during the mission. The highest chance of occurring is related to events with fluences between 10^6 and 10^7 protons/cm^2. In order to estimate the count rate on the LISA silicon telescopes generated by SEPs associated to evolving CMEs as a function of time we have

considered three events: May 7th 1978 (Grieder, 2001), February 16th 1984 (Zhang et al., 1993), and September 29th, 1989 (Cramp, Duldig and Humble, 1993). These flares produced SEP fluences of more than 10^6 protons/cm^2, about 10^7 protons/cm^2 and 10^9 protons/cm^2, respectively.

In figs. 15, 16 and 17 we have reported the solar proton spectra reaching the Earth as a function of time during the May 7th, 1978, February 16th 1984, and September 29th, 1989 flares, respectively.

In figs. 15 and 16 the proton fluxes have been divided by various factors in order not to superimpose all lines. In figs. 15, 16 and 17 the SEP spectra observed as a function of time have been compared to the peak fluxes of various fluence gradual events according to the modelization by M&N (dotted lines). The peak flux trend of the model results in a quite good agreement with peak SEP flux measurements. It is extremely interesting to notice as the particle spectra show fast changing trends before reaching the peak flux in figs. 15 and 17.

In fig. 18 we have reported the results presented by Sokolov et al., 2004, where upstream proton spectra at 1 AU as a function of time are shown. The curves have been calculated at intervals of time of 0.5 hours (the bottom curve corresponds to t=0; the top one at t=3.5 hours). The shock position was assumed at 20 solar radii from the Sun. A comparison is made with the proton fluxes observed as a function of time during the May 7th 1978 flare event where no normalization factors were considered.

The galactic cosmic-ray proton flux at solar minimum and maximum (continuous and dashed lines, respectively) have also been shown in figs 15 to 17. The galactic cosmic-ray parameterization near the LISA orbit has been discussed in Grimani et al., 2004. In particular, the proton flux has been fitted as it follows:

$$18000(E+1.09)^{-3.66}E^{0.87}Part/(m^2srsGeV) \tag{6}$$

$$18000(E+1.55)^{-3.90}E^{1.11}Part/(m^2srsGeV) \tag{7}$$

at solar minimum and maximum, respectively.

SEP fluxes have been parameterized by using power-law functions in proper subintervals of energy.

We have determined the integral fluxes in energy above 100 MeV.

For primary cosmic rays we have found an integral flux of 0.335 protons/(cm^2 sr s) and 0.150 protons/(cm^2 sr s) at solar minimum and maximum, respectively.

In Tables 3 and 4 we have reported the results of the energy integral SEP and upstream proton fluxes, respectively. The fluxes are numbered as in figs. 15, 16, 17 and 18.

Table 3: SEP energy integral fluxes of various fluence events. Fluxes are numbered as in figs. 15, 16 and 17.

	Flux number	Integral flux (protons/(cm^2 sr s))
Flare May 7th 1989	Flux 1	1.01
	Flux 2	5.22
	Flux 3	8.26
	Flux 4	10.60
	Flux 5	10.96
Flare February 16th 1984	Flux 1	20.33
	Flux 2	28.60
	Flux 3	27.24
	Flux 4	48.32
Flare September 29th 1989	Flux 1	0.435
	Flux 2	106.88
	Flux 3	392.72

7.4 LISA particle monitors expected response to SEPs

In paragraph 6 we have reported the characteristics of the silicon detectors used as particle counters. In order to show how the count rate is expected to change at the passage of a CME, we report firstly the expected count rate due to incident galactic protons at solar minimum and maximum, respectively. We are assuming that no protons with energies smaller than 100 MeV will go through the silicon detectors.

The geometrical factor of one detector only is 9.24 cm^2 sr, when an isotropic flux of incident particles from above and below is considered. On the basis of

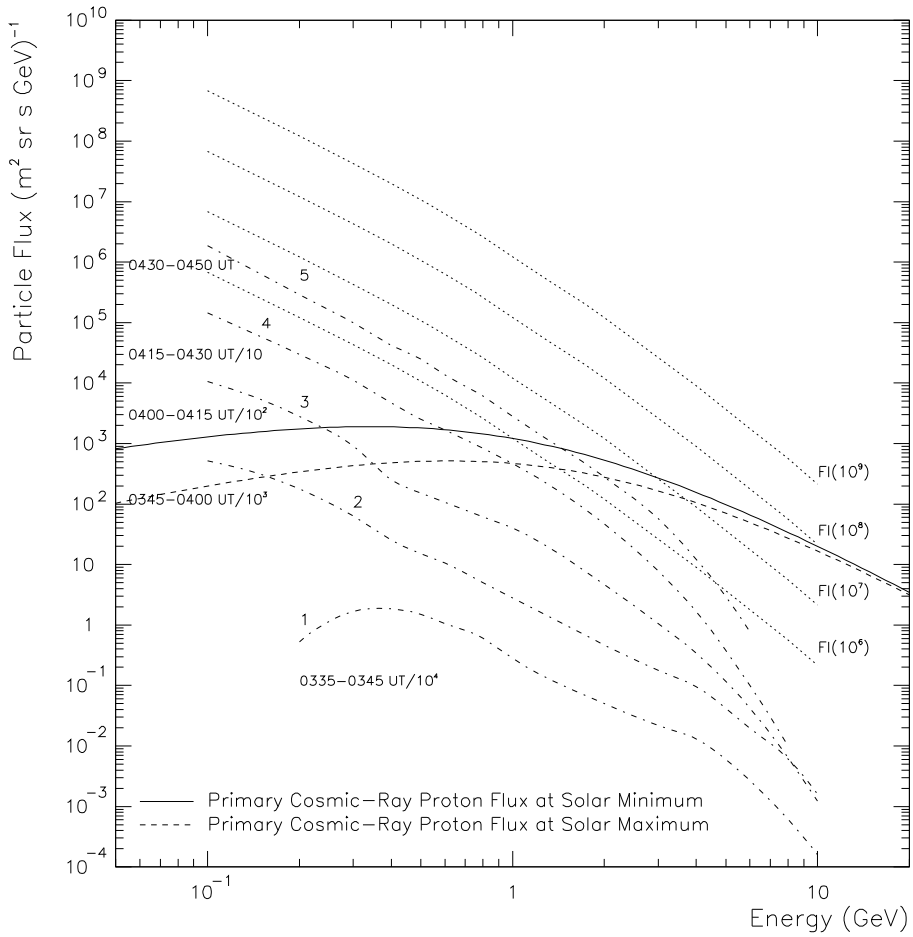

Figure 15: Solar proton spectra reaching the Earth as a function of time during the May 7th 1978 flare (dot-dashed lines). The dotted lines represent various fluence peak fluxes generated by SEPs in units of protons/cm^2. The continuous and dashed lines correspond to primary cosmic-ray proton fluxes at solar minimum and maximum, respectively. See text for more details.

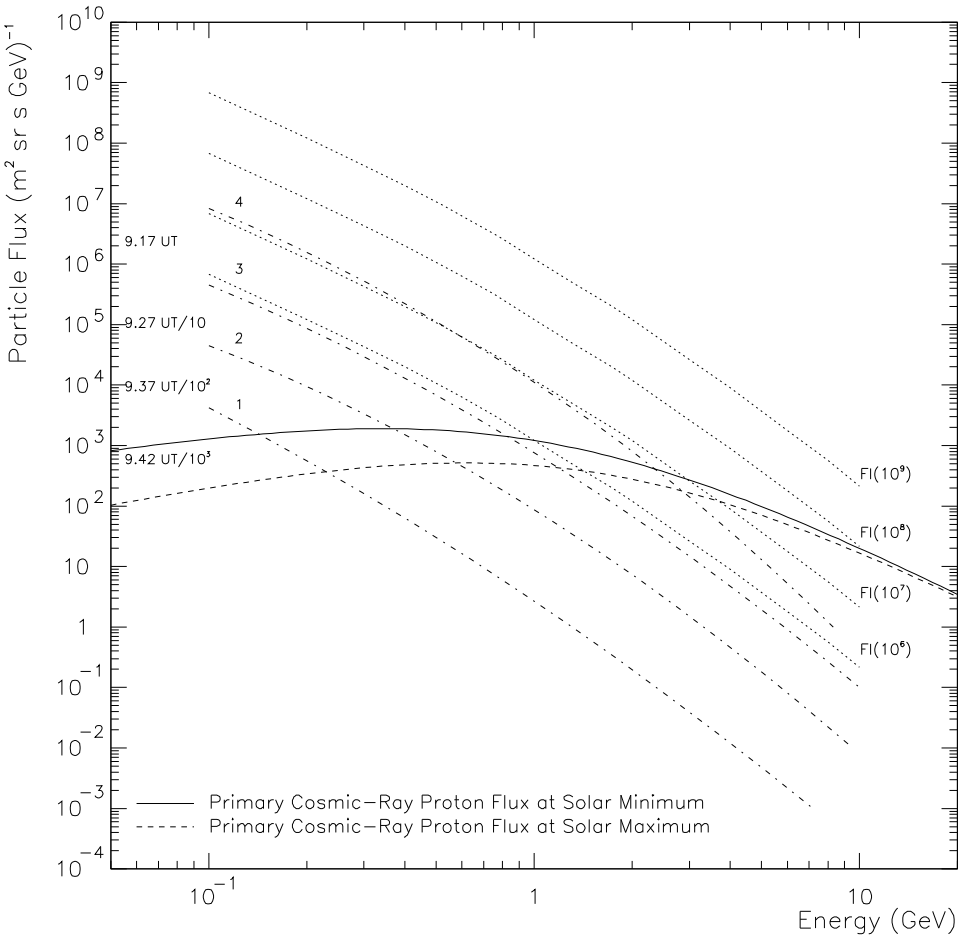

Figure 16: Solar proton spectra reaching the Earth as a function of time during the February 16th 1984 flare (dot-dashed lines).The dotted lines represent various fluence peak fluxes generated by SEPs in units of protons/cm^2. The continuous and dashed lines correspond to primary cosmic-ray proton flux at solar minimum and maximum, respectively. See text for more details.

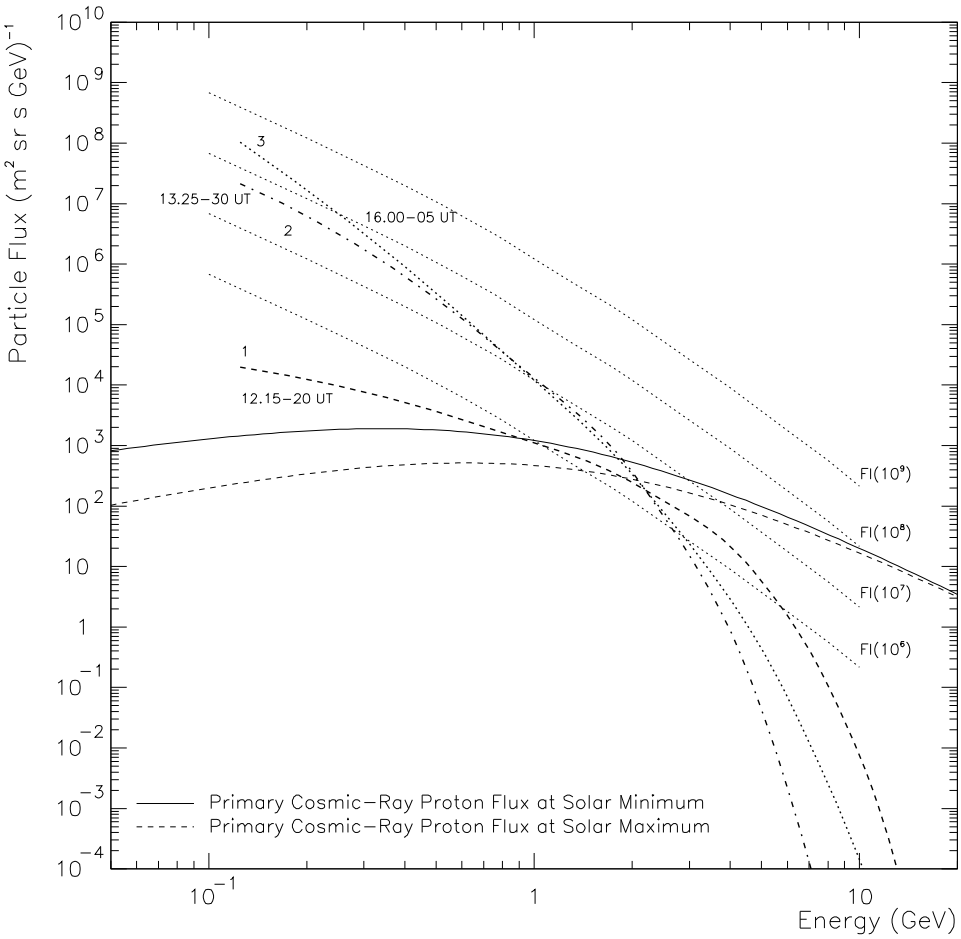

Figure 17: Solar proton spectra reaching the Earth as a function of time during the September 29th 1989 flare (thick lines).The dotted lines represent various fluence peak fluxes generated by SEPs. The continuous and dashed lines correspond to primary cosmic-ray proton fluxes at solar minimum and maximum, respectively. See text for more details.

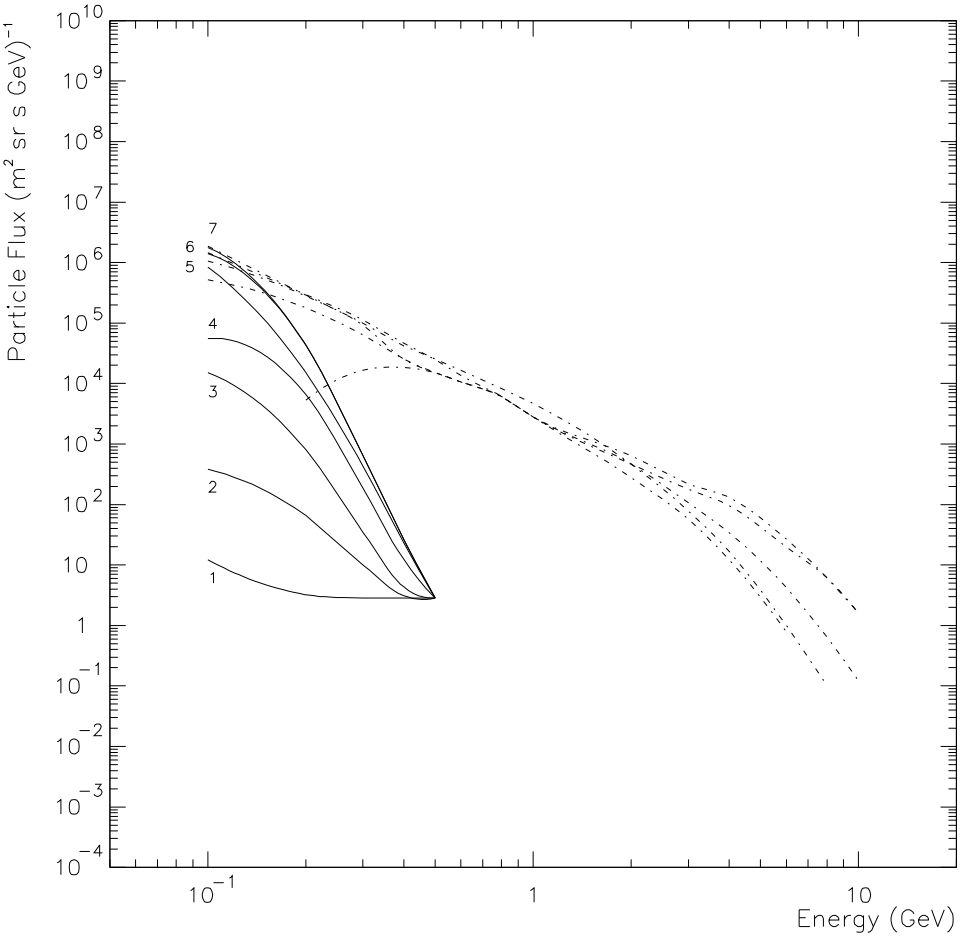

Figure 18: Solar proton spectra reaching the Earth as a function of time during the May 7th 1978 flare (dot-dashed lines). Calculated time sequence of upstream differential proton intensity at the distance of 1 AU (continuos lines) are also shown with no normalization scaling (Sokolov et al., 2004). The time interval between two adjacent continuous curves is 30 minutes. The bottom curve corresponds to t_o and the top one to t_1=t_o+3.5 hr. The shock position was assumed at 20 solar radii.

Table 4: Upstream proton integral fluxes. Flux numbers are indicated as in Fig. 18

Flux number	Integral Flux (protons/(cm^2 sr s))
Flux 1	2.01×10^{-4}
Flux 2	22.67×10^{-4}
Flux 3	548.50×10^{-4}
Flux 4	0.3004
Flux 5	1.822
Flux 6	4.653
Flux 7	5.072

the same assumptions the geometrical factor of the 'double' configuration is 0.872 cm^2 sr. The resulting count rates at solar minimum and maximum are reported in Tables 5 and 6. Only one tenth of events go through both silicon detectors compared to those traversing only one layer.

Table 5: Expected particle monitor count rate at solar minimum due to primary protons

Detector configuration	Count rate (protons/s)
Top detector only	3.1
Double configuration	0.292

Table 6: Expected particle monitor count rate due to primary protons at solar maximum

Detector configuration	Count rate (protons/s)
Top detector only	1.39
Double configuration	0.131

Solar particles move preferentially along the interplanetary magnetic field lines. However, while CMEs propagate the magnetic field is distorted. We will assume here that SEPs also present an isotropic incident flux on particle

monitors. Consequently, the same geometrical factors for the silicon telescopes have been considered for incident galactic and solar protons.

The particle detector count rates expected in one and both planes of silicon wafers at the passage of various fluence solar events is reported in Tables 7 and 8. ¿From a comparison with Tables 5 and 6 it can be noticed that strong solar events may increase the count rate of the silicon detectors between one and three orders of magnitude with respect to the primary cosmic-ray background.

Please note that the Flux 3 of the September 29th 1989 flare would generate a calculated count rate of 3628 protons/s. This count rate corresponds to an incident flux larger than 10^8 protons/cm^2 expected to cause saturation of the silicon detectors.

In Table 9 the expected count rates generated by upstream proton spectra is presented for comparison.

Table 7: Expected count rate in one plane of the silicon detector due to various fluence solar events

	Flux number	Count rate (protons/s)
Flare May 7th 1989	Flux 1	9.36
	Flux 2	48.24
	Flux 3	76.30
	Flux 4	97.94
	Flux 5	101.27
Flare February 16th 1984	Flux 1	187.85
	Flux 2	264.26
	Flux 3	251.70
	Flux 4	446.48
Flare September 29th 1989	Flux 1	4.023
	Flux 2	987.57
	Flux 3	- (3628.73)

7.5 Solar energetic particle mapping

In this paragraph we illustrate possible, reasonable scenarios about expected count rate variation on the silicon telescopes from steady-state at solar maximum to the transit of SEPs through the LISA spacecraft. PHOEBUS will allow us three observation points separated by 2 degrees in longitude.

Table 8: Count rate on both planes of the particle counters (double configuration) due to various fluence solar events

	Flux number	Count rate (protons/s)
Flare May 7th 1989	Flux 1	0.884
	Flux 2	4.56
	Flux 3	7.20
	Flux 4	9.243
	Flux 5	9.557
Flare February 16th 1984	Flux 1	17.73
	Flux 2	24.94
	Flux 3	23.75
	Flux 4	42.13
Flare September 29th 1989	Flux 1	0.40
	Flux 2	93.20
	Flux 3	342.45

Table 9: Expected count rate on one plane and both planes (double configuration) of the particle counters due to upstream proton fluxes. The fluxes have the same meaning of fig. 18

Flux number	Count rate on one silicon layer (protons/s)	Count rate on both silicon layers (protons/s)
Flux 1	1.854×10^{-3}	1.750×10^{-4}
Flux 2	0.0209	1.977×10^{-3}
Flux 3	0.5068	0.0478
Flux 4	2.776	0.2619
Flux 5	16.831	1.588
Flux 6	42.997	4.058
Flux 7	46.864	4.423

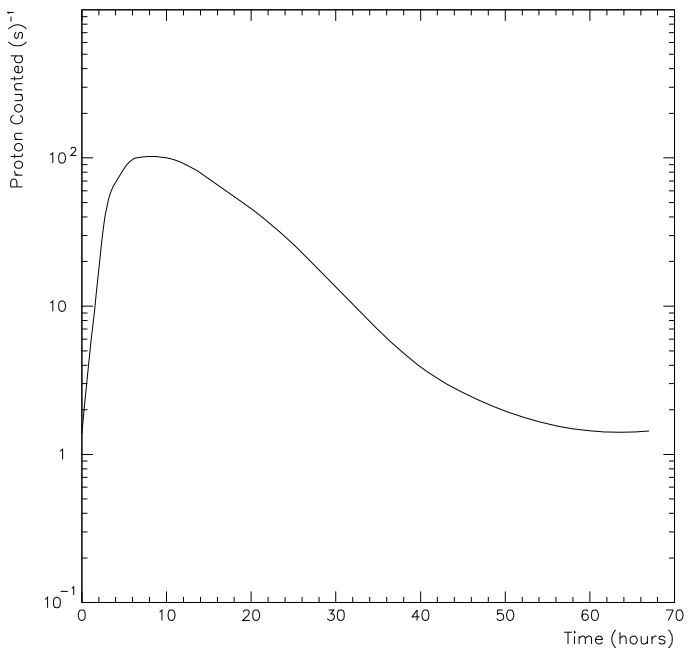

Figure 19: Expected count rate variation on the PHOEBUS particle telescopes on LISA for a typical western event.

We won't make any guess at this stage about different count rates on the three LISA spacecraft.

Our data will be possibly compared to observations of other experiments in space. Strong shocks accelerating particles above 1 GeV present velocities larger than 1500 km/s (Reames, Barbier & Ng 1996). Consequently, shocks take two days, tipically, to reach LISA or Earth from the Sun.

In case of a western event with respect to the LISA-Earth system, a pretty sudden increase on the counters is expected to be followed by a slow decrease of the order of a couple of days. Conversely, a central-eastern event will appear as an increase of the particle counts then a plateau, a maximum at the shock transit and a slow decrease. In figs. 19 and 20 we have reported the proton count rates possibly observed at the LISA spacecraft for a western and a central-eastern event, respectively.

The particle monitor count rate is dominated by the low energy part of the incident proton spectra with a sudden increase at the peak transit. In order to develop a model of SEP dynamics it will be important to add the

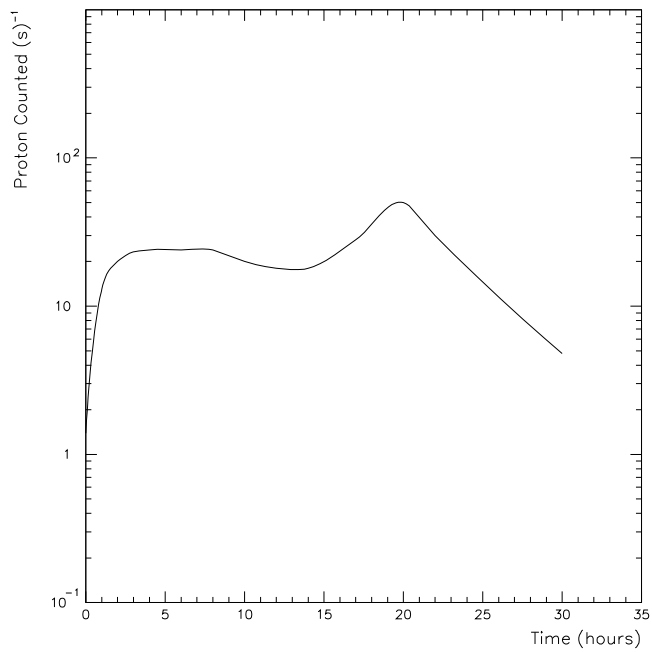

Figure 20: Expected count rate variation on the PHOEBUS telescopes on LISA for a typical central-eastern event.

proton spectra data up to a few hundreds of MeV to the count rate. For the PHOEBUS proton spectrum analysis capabilities see Araújo & Wess, 2004.

The LISA Pathfinder mission, even if it is supposed to take data during a period of solar minimum, will offer the possibility to verify our steady-state predictions for incoming galactic cosmic rays and, eventually, in case of SEP detections. We will have also the possibility to compare the data gathered by the silicon telescope on board the Pathfinder to other experiment observations.

8 Space weather

8.1 Introduction

Space Weather has been defined as the observation, study and forecasting of solar activities and their effect on the solar wind, the magnetosphere and the ionosphere which have the potential to affect the near Earth environment.

Moving beyond the Earth's atmosphere and magnetosphere that act as protective shields, we are exposed to sources of radiation that can be a serious

hazard for life and machines.

Dramatic solar activity can affect a large number of man-made systems (Albertson et al., 1992). Some of the earliest examples of the impact of electric and magnetic disturbances of the upper atmosphere on terrestrial systems were given by telegraph operators. During large solar disturbances telegraph lines sometimes appeared to be non-operable or operable without a battery supply (Lanzerotti, 1979).

More recently one of the most extreme examples is the failure of the Quebec Hydro's power system. A geomagnetic storm at 2:45 on March 13, 1989 tripped five 735 kV lines from James Bay causing a generation loss of 9450 MW.

The ionospheric currents during a storm, generated when bursts of plasma ejected from the Sun investe the Earth, can reach tens of thousands of amperes (Aspnes et al., 1989) and produce fluctuations in the Earth's magnetic field. As stated by Faraday's law, a time-changing magnetic field will induce an electric potential on conductors. During a geomagnetic storm a potential of up to 1 V/km can be induced on the Earth's surface, which is a spherical conductor (Akasofu and Aspnes, 1982). In response to potential differences between two locations on the ground, an electric current is induced in conductors within the Earth's surface (Aspnes et al., 1989; Albertson et al., 1992). The potential differences persist for minutes resulting in slowly oscillating currents of tens to hundreds of amperes (Ringlee and Stewart, 1989).

As more and more advanced electric and magnetic apparata are employed in every-day activities, the effects of the upper atmosphere become more important. Today there are a large number of man-made systems that are affected by geomagnetic storms.

Examples are the following:

Satellite Systems: when the number and energy of the impacting particles increases, the operation of the satellite can be affected adversely and can induce command and data modifications or lead to satellite surface charging problems degrading the lifetime of the satellite and affecting the electronics.

Communication Systems: strong magnetic storms can affect radio waves propagation characteristics and lead to depression in the maximum usable communication frequencies.

Power Systems: transmission lines are potentially very good conductors of geomagnetic induced currents, and their flow through power system transformers to ground is the main problem during a storm.

Navigation Systems: the accuracy of navigation systems using very low frequency signals depends on accurately knowing the altitude of the ionosphere's lower boundary. During a geomagnetic storm the altitude of the ionosphere changes rapidly and can introduce errors of several kilometers.

Human Exposure: increased radiation exposure to astronauts and airplane crew and passengers on polar routes can be lethal.

Only a complete understanding of solar variability is enabling us to address the issues of Space Weather and their predictability.

8.2 Space weather with LISA

Large 'gradual' SEP events occur at a rate of 10 - 20 yr^{-1}, those able to endanger to human life occur less than once per decade. For this reason it is especially difficult to study or to predict them. CME speed is the best predictor of intense SEP events.

As described in the previous paragraphs, shock peak intensity are produced by evolving CMEs from central meridian that produce sufficiently fast shocks to continue acceleration out to 1 AU. Shock peaks involving protons with energy greater than 100 MeV can be a serious risk when they occur. In particular, the level of hazard depends on the flux trend at the *knee* as it can be observed from the two proton spectra reported in fig.21. The levels of radiation hazard to astronauts outside the magnetosphere is also shown. *Soft* radiation occurs where protons begin to penetrate space suits or spacecraft walls. *Hard* radiation refers to protons that can penetrate $\simeq$ 5 cm of Al: at this stage shielding becomes impractical. Even if the two events reported in fig.21 have similar proton intensities from 10 to 100 MeV, the different values of E_{knee} cause vastly different levels of hazard. The spectrum shown for the 1989 September event would produce $\simeq 4\ rem\ hr^{-1}$ behind 10 $g\ cm^{-2}$ of shielding (Reames 2000). The dose allowed per year for the astronauts is 50 rem, and it would be accumulated with half a day of exposure to such intensities. A truly serious situation would result if a high-energy knee persisted

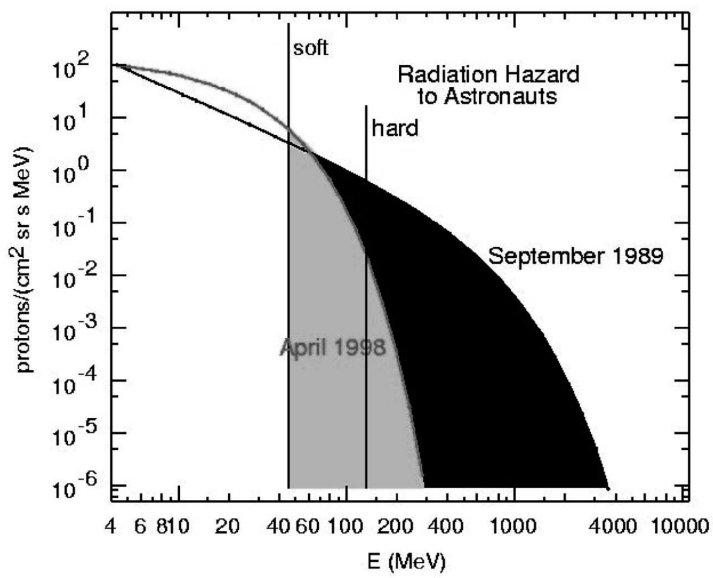

Figure 21: Astronaut radiation hazard due to different E_{knee} SEP fluxes. Figure is taken from Reames, 2000.

until the large peak at the time of the shock passage. The event of 1972 August 4th is an example of high intensities of high-energy protons occurring at a shock peak; unfortunately, instrument saturation prevented definitive spectral measurements for that event. It is generally accepted that radiation levels in the 1972 August 4th event would have been fatal to inadequately shielded astronauts. The issue is the thickness of shielding required for protection. The thickness required to stop protons of given energy goes as the 1.6 power of the energy. Increasing E_{knee} from 50 to 500 MeV would increase the thickness and weight of the required shielding by a factor of 40. Mission costs increase at least linearly with payload weight.

Moreover the position of the three LISA spacecraft (see fig.9) could be ideal to predict in advance the passage of some SEP events at the Earth. In fact, shocks whose nose traverses LISA and consequently invests the Earth on the west flank will be detected before their passage at the Earth.

9 Network with other space weather experiments

The Solar Probe and Solar Orbiter experiments are supposed to be launched during the LISA mission (2012-2015). Solar Probe will pass near the Sun (polar orbit, 4 Sun radii distance) at different times of the solar cycle. It will investigate processes heating the corona and accelerating solar wind particles. Solar Orbiter will study the Sun from 0.21 AU. It will investigate particle acceleration from coronal holes, streamers, CMEs and associated shocks, active regions and flare location. It will be of great interest to compare the results of these experiments to the PHOEBUS data.

10 Fake gravitational wave signals induced by CMEs

Since the rotation motion of the LISA spacecraft on an equilateral triangle is slow compared to the time needed to SEPs associated to an evolving CME to traverse the LISA experiment and since the particles are strongly constrained to follow the interplanetary magnetic field lines, the particle detectors on LISA are, in general, interested by the solar particle flux increase at different times.

In principle, various scenarios must be considered in case nose, flanks or shock passage interest the LISA detectors.

The solar particle incident fluxes change very rapidly at the shock passage while they remain pretty stable and high in the nose region and stable and low in the invariant spectral region.

As a consequence, a series of signals of frequency below a few units 10^{-4} Hz might be generated on the spacecraft as a result of the onset on each detector and the variation of the solar particle fluxes.

The signals generated by expanding CMEs while traversing the LISA spacecraft should be compared to the simulations of the expected gravitational wave signals produced by genuine sources.

Acknowledges

The authors are very grateful to Dr. Maurizio Candidi, Dr. Marisa Storini of the IFSI/CNR - Italy, Prof. Ester Antonucci of the University of Turin, Prof. Maurizio Busso of the University of Perugia and to Dr. Eamonn Daly (Space Environments and Effects Analysis Section - ESA) for having supported and encouraged this work. A special thank to Prof. B. Sanahuja and Dr. A. Aran of the University of Barcelona and to Prof. M. Panasyuk, Prof. R. A. Nymmik and Pr. V. N. Mileev of the Skobeltsyn Institute of Nuclear Physics of Lomonosov, Moscow University for very useful discussions and suggestions regarding this project.

References

Albertson, V. D. et al., 1992, IEEE Transactions on Power Delivery, 8, 1206

Akasofu, S. I. and Aspnes, J. D., 1982, Nature, 295, 136

Aran, A., Sanahuja, B. & Lario, D., Final Report ESA/ESTEC (Contract 14098199/NL/MM) http://www.am.ub.es/ blai

Araújo, H. M. & Wess, P., 2004, LISA coll. internal note

Araújo, H. M. et al., 2004, Astrop. Phys. in press, Preprint astro-ph/0405522

Aspnes, J. D., Merritt, R. P., Spell, B. D., 1989, IEEE Power Engineering Review, 9, 10

Cramp, J. L., Duldig, M. L. & Humble, J. E., 1993, Proc. Int. Cosm. Ray Conf., Calgary, 3, 47

Dalla, S. et al., 2003, Geophys. Res. Lett., 30, 8035

Grieder, P. K. F., 2001, Cosmic Rays at the Earth, Elsevier Science, Ed.

Grimani, C. et al., 2002, A&A, 392, 287

Grimani, C. et al., 2004, Class. Quant. Grav., 21, S629

Grimani, C. et al., 2005, to appear on Class. Quant. Grav.

Grimani, C. & Vocca, H., 2005, to appear on Class. Quant. Grav.

Lanzerotti, L. J., Journal of Atmospheric and Terrestrial Physics, 1979, 41, 787

Kahler, S.W., 1994, Ap.J., 428, 837

Karpov, S. N., Miroshinechenko, L. & Vos, 1997, Proc. Int. Cosmic Ray Conf., Durban, 1, 205

Lobo, A., 2004, DDS Science requirements DDS-IEEEC-ScRD Draft issue

Lovell, J. L., Duldig, M. L., and Humble, J. E., 1998, J. Geophys. Res. 103, 23, 733

McKibben, R. B. et al., 2003, Annals Geophysical, 21, 1217

Mottl, D. A. & Nymmik, R. A., 2002, Sub. Adv. Space Res.

Nymmik, R. A., 1999, Proc. 25th Int. Cosm. Ray Conf., Salt Lake City, 6, 268

Pallavicini, R., Seno, S. & Vaiano, G. S., 1977, Ap. J., 216, 108

Reames, D. V., Barbier, L. M. & Ng, C. K., 1996, Ap. J., 466, 473

Reames, D. V., Kahler, S. W. & Ng, C. K., 1997, Ap. J., 491, 414

Reames, D. V., 1999, Space Sci. Revs., 90, 413

Reames, D. V., 2000, SEPs: Space Weather Hazard in Interplanetary Space, Chapman Conference, Space Weather: Progress and Challenges in Research and Applications, Clearwater, FL, March 20-24

Reames, D. V., 2001, Space Weather Eds. P. Song, H. J. Singer and G. Siscoe, Geophysical Monograph 125 (AGU, Washington DC), p. 101

Reames, D. V., 2002, Solar Energetic Particles, Adv. Sp. Res.

Reames, D. V., 2003, Solar Energetic Particle Variations, Adv, Sp. Res.

Ringlee, R. J. & Stewart, J. R., 1989, IEEE Power Engineering Review, 9, 6

Shea, M. A. & Smart, D. F. 2001, Proc. Int. Cosm. Ray Conf., Hamburg, 3401

Smart, D. F. & Shea, M. A. 1996, Adv. Space Res., 17, 116.

Sokolov, I. V., 2004, Ap. J. Lett., 616, L171

Stephens, S. A. & Streitmatter R. E., 2001, Adv. Sp. Res., 27, 749

Tylka, A. J., D. V. Reames, and C. K. Ng, 1999, Geophys. Res. Letters, 26, 2141

Tylka, A. J.et al., AIP Conf. Proc., 2000, 528, 147

Vocca, H. et al., 2004, Class. Quantum Grav., 21, S665

Vocca, H. et al., 2005, to appear on Class Quant. Grav.

Wess,P., Araújo, H. M. & Sumner, T. J., Lisa collaboration internal note, 12 May 2003, Charging process of the LISA test masses

Wheatland, M. S., 2000, Ap. J. Lett., 536, L109

Zhang, Li et al., 1993, 23rd Proc. Int. Cosmic Ray Conf., Calgary, 3,37